J Oceanogr (2015) 71:663–673
DOI 10.1007/s10872-015-0305-5

ORIGINAL ARTICLE

A long-term volume transport time series estimated by combining in situ observation and satellite altimeter data in the northern South China Sea

Xiao-Hua Zhu[1,3] · Ruixiang Zhao[1] · Xinyu Guo[1,2] · Yu Long[1] · Yun-Long Ma[1] · Xiaopeng Fan[1]

Received: 9 March 2015 / Revised: 1 June 2015 / Accepted: 4 June 2015 / Published online: 26 June 2015

Abstract We deployed five pressure-recording inverted echo sounders (PIES) along a satellite altimeter track across the continental slope of the northern South China Sea (NSCS) from October 2012 to July 2014, and obtained a time series of volume transport (VT_{PIES}) across the section from their records. Applying the empirical relationship between VT_{PIES} and the satellite altimeter sea surface height anomaly difference across the section, we obtained a time series of volume transport (VT_{NSCS}) over 22 years from 1992 to 2014. The VT_{NSCS} shows a small mean value of −1.6 Sv (1 Sv = 10^6 m^3 s^{-1}) (i.e., toward the southwest), but a significant seasonal reversal and mesoscale eddy induced fluctuations (−11.8 to 19.7 Sv). The monthly mean of VT_{NSCS} over 22 years shows a maximum (3.6 Sv) in July and a minimum (−7.3 Sv) in December. This is the first long time series of volume transport for the NSCS based on in situ data.

Keywords Long-term time series of volume transport · Pressure-recording inverted echo sounder · Gravest empirical mode · Satellite altimeter · Seasonal variability · South China sea

✉ Xiao-Hua Zhu
xhzhu@sio.org.cn

[1] State Key Laboratory of Satellite Ocean Environment Dynamics, Second Institute of Oceanography, State Oceanic Administration, 36 Baochubei Road, Hangzhou 310012, China

[2] Center for Marine Environmental Study, Ehime University, 2-5 Bunkyo-cho, Matsuyama 790-8577, Japan

[3] Ocean College, Zhejiang University, Hangzhou 310058, China

1 Introduction

The South China Sea (SCS) is located at the west side of the North Pacific and is the largest semi-enclosed marginal sea of the North Pacific Ocean, with a wide continental shelf and slope along the mainland coast of southern China. The upper layer large-scale circulation is predominantly seasonal, not only changing its magnitude, but also reversing direction, mainly because of the Asian monsoon seasonal cycle (Wyrtki 1961; Liu et al. 2001). The basin scale circulation pattern of the SCS has been investigated in many studies incorporating in situ measurements (e.g., Wyrtki 1961; Fang et al. 2002), satellite-based observations (Wu et al. 1998), as well as numerical simulations (Wang et al. 2006). During boreal winter, the basin scale cyclonic gyre forms a strong southwestward current known as the SCS western boundary current, flowing along the southern China continental slope and eastern Vietnam coast from Dosha Island to the region south of Vietnam. During boreal summer, the SCS western boundary current in the northern SCS (NSCS) becomes weak and variable, and needs further clarification (Fang et al. 2012).

On the other hand, deep, cold, and salty Philippine Sea water enters the SCS through the Luzon Strait and then flows out through the Taiwan, Karimata, and Mindoro Straits as shallow warm currents. This current system, a heat and freshwater conveyor, is called the South China Sea throughflow (Qu et al. 2006). During the past several decades, many investigations have produced widely varying estimates of the net volume transport through the Luzon Strait, from 0.5 to 10 Sv (1 Sv = 10^6 m^3 s^{-1}) (e.g., Wyrtki 1961; Hsin et al. 2012). Mean net volume transport through the Taiwan Strait is about 1 Sv in winter and 2–3 Sv in summer (Fang et al. 2009; Hu et al. 2010). The mean outflow transports through the Karimata and Mindoro

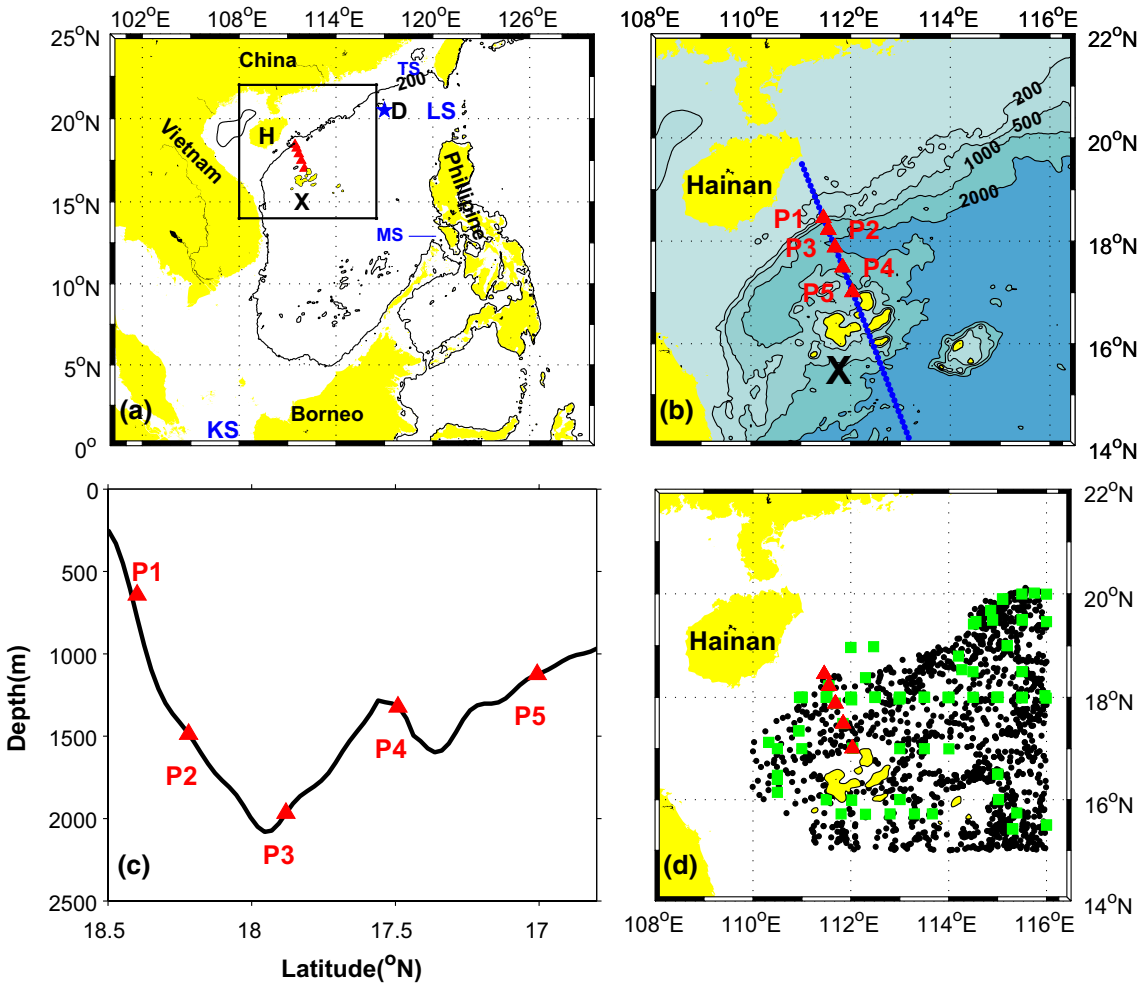

Fig. 1 **a** The South China Sea (SCS) and its adjacent seas; 200 m isobaths denotes the position of shelf slope along which the SCS western boundary current flows, **b** detailed map of the observational site, **c** vertical cross-section view of bottom topography along the mooring array, **d** positions of hydrocasts used in computing the GEM. The TOPEX/POSEIDON and Jason-1/2 satellite altimeter track (Pass 114) is indicated with *blue dots* in **b**. *Red triangles* (P1, P2, P3, P4, and P5) indicate the locations of the five PIESs. The *black dots* and *green squares* indicate the positions of Argo profiles and CTD casts, respectively. "H" and "X" in **a** and **b** indicate Hainan Island and Xisha Island, respectively. "TS", "LS", "MS", and "KS" in **a** indicate Taiwan Strait, Luzon Strait, Mindoro Strait, and Karimata Strait, respectively. Isobath depths are given in meters (color figure online)

Straits are, respectively, given as 3.6 Sv in boreal winter (Fang et al. 2010) and 2.4 Sv during 2004–2007 (Qu and Song 2009). However, by comparison with these transport estimates through the straits around the SCS, transport estimates in the inner SCS are very scarce. To date, there have been no volume transport time series based on in situ observations in the SCS.

In this study, we carried out a 22-month mooring deployment of five pressure-recording inverted echo sounders (PIES) in the NSCS to obtain a 22-month-long record of volume transport across the mooring array. We then estimated a 22-year-long volume transport time series by developing and using an empirical relationship between the observed volume transport and satellite altimeter-determined sea surface height anomaly difference and investigated its mean and variability, including the seasonal cycle and fluctuations induced by mesoscale eddies.

2 Data and methods

We deployed an array of five PIESs across the continental slope in the NSCS, along a satellite track (Pass114) of the TOPEX/POSEIDON and Jason-1/2 altimeters in October 2012, and maintained it until July 2014 (Fig. 1a, b). This PIES array crosses over the gap between Hainan Island and Xisha Island (Fig. 1b, c). The PIES array is roughly perpendicular to the bathymetry contours of the continental slope, i.e., the western boundary current in the NSCS, assuming the current flows along isobaths over the continental slope.

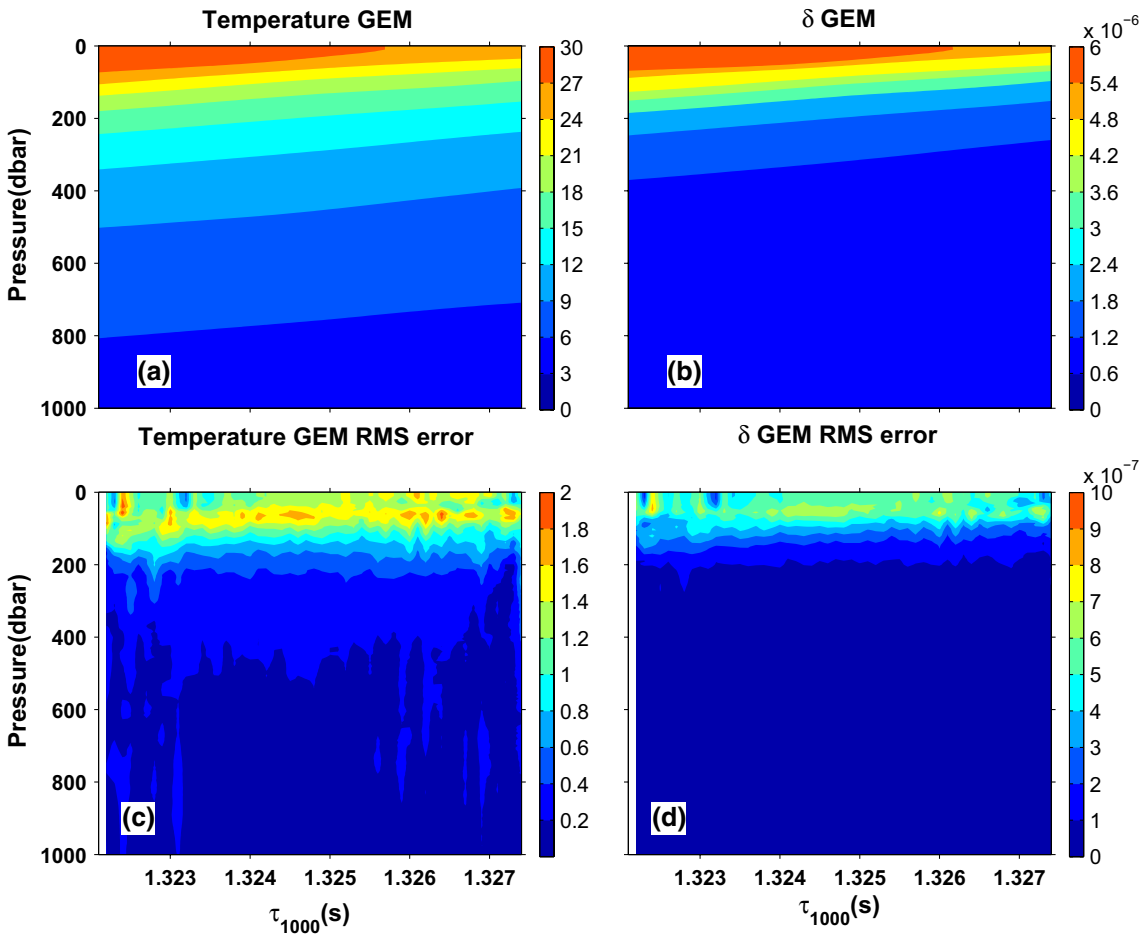

Fig. 2 Temperature (°C) and specific volume anomaly ($m^3\ kg^{-1}$) GEM (*upper panels*) and their errors (*bottom panels*)

While the PIESs were making measurements, we performed a ship-mounted acoustic Doppler current profilers (ADCP, RDI-VM38, 38.4 kHz) survey along the PIES array and took five conductance–temperature–depth (CTD) casts at the PIES stations during 15–16 December 2012, to get data for comparison with the PIES mooring data.

The PIES measures the round-trip acoustic travel time (τ) between sea surface and bottom and the near-bottom pressure (P_b). The τ measurements were used to estimate vertical profiles of temperature and specific volume anomaly by the gravest empirical mode (GEM) method (Watts et al. 2001; Zhu et al. 2003; Andres et al. 2008b) using 1355 profiles of temperature and salinity obtained by CTD and Argo measurements (Fig. 1d). The GEM errors for temperature (specific volume anomaly) are 0.77 °C ($2.41 \times 10^{-7}\ m^3\ kg^{-1}$) in the upper 300 m layer and 0.15 °C ($6.51 \times 10^{-8}\ m^3\ kg^{-1}$) for a full-depth layer, respectively (Fig. 2). The GEM-inferred temperatures on 16 December 2012 are in good agreement with those independent data measured by the

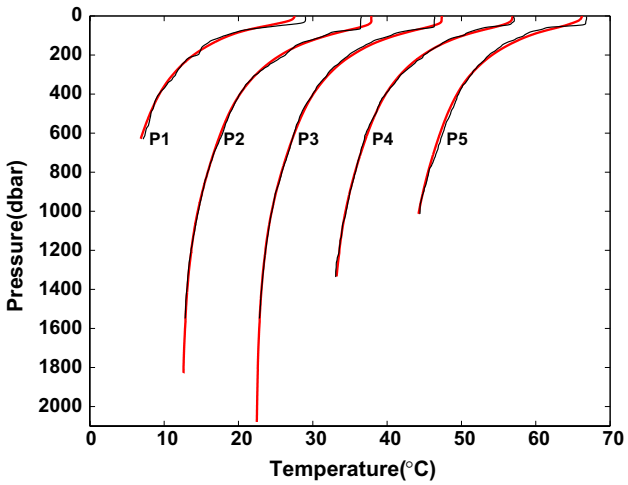

Fig. 3 Temperature profiles obtained from CTD measurements (*black*) and the GEM at five PIES sites. The temperature profiles for P2–P5 stations have been offset rightward by 10 °C successively

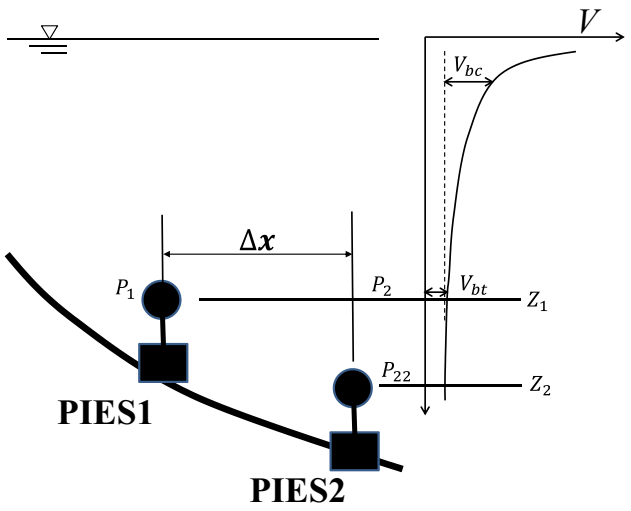

Fig. 4 Diagram (not to scale) of terms used in Eqs. (1)–(4)

CTD casts at the five PIES stations during our cruise. Root-mean-square differences (RMSDs) between the two measurements are 0.76 °C in the upper 300 m layer and 0.29 °C for a full-depth layer, respectively (Fig. 3). This indicates the measurements of τ provide good proxy for estimation of the vertical profiles of temperature by the GEM method.

Each P_b record is processed to remove the tide and sensor drift for estimating the barotropic velocity between station pairs as follows (Donohue et al. 2010). Absolute geostrophic velocity (V) relative to a deep reference level includes both barotropic component (V_{bt}) and baroclinic component (V_{bc}) (Fig. 4):

$$V = V_{bc} + V_{bt} \tag{1}$$

The V_{bc} can be calculated from the PIES-measured τ data using the GEM-derived specific volume anomalies. The V_{bt} at level Z can be calculated from the pressure gradient between two stations:

$$V_{bt} = (p_1 - p_2)/(\Delta x f \rho) \tag{2}$$

where p_1 and p_2 are pressures at level Z1 from two stations, ρ is density, f is the Coriolis parameter (5.0×10^{-5} s^{-1}), and Δx is the distance between two stations (Fig. 4).

Since p_1 and p_2 are not always measured at the same depth, we need to use pressure records at different depth to calculate barotropic component. For this purpose, V_{bt} is divided into the temporal mean ($\overline{V}_{bt}$) and its deviation ($V'_{bt}(t)$):

$$V_{bt}(t) = \overline{V}_{bt} + V'_{bt}(t) \tag{3}$$

The $V'_{bt}(t)$ can be rewritten as:

$$V'_{bt}(t) = \left(p'_1(t) - p'_2(t)\right)/(\Delta x f \rho) \approx \left(p'_1(t) - p'_{22}(t)\right)/(\Delta x f \rho) \tag{4}$$

by assuming the temporal variation of deep pressure is small ($p_2' \approx p_{22}'$) (see Fig. 4 for definition of p_{22}'). p_1' and p_{22}' can be obtained from the PIES pressure measurements at the two stations.

The velocity measured by the ship-mounted ADCP at a deep layer (800 m) and averaged between two stations, including both barotropic and baroclinic components, should be the same as that estimated by the PIES data:

$$V_{ADCP} = \overline{V}_{bt} + V'_{bt}(t_{ADCP}) + V_{bc}(t_{ADCP}) \tag{5}$$

where t_{ADCP} denotes the time of ADCP measurement. Therefore, the temporal-mean barotropic component $\overline{V}_{bt}$ can be estimated as follows:

$$\overline{V}_{bt} = V_{ADCP} - V'_{bt}(t_{ADCP}) - V_{bc}(t_{ADCP}) \tag{6}$$

$V'_{bt}(t_{ADCP})$ can be estimated by applying Eq. (4) to P_b while $V_{bc}(t_{ADCP})$ by using the GEM-derived hydrographic data during the period of the ship-mounted ADCP measurement, respectively. The resulting $\overline{V}_{bt}$ at the four station pairs was within a range between −1.0 and 1.5 cm s^{-1}. Substituting $\overline{V}_{bt}$ given by Eq. (6) into Eq. (3) and estimating $V'_{bt}(t)$ from records of P_b and V_{bc} from records of τ, we obtained the absolute geostrophic velocity and corresponding volume transport through the mooring section.

3 Results

3.1 Velocity structure

The vertical cross-section of the current velocity obtained by the ship-mounted ADCP measurements on 16 December 2012 shows a southwestward current with a subsurface maximum velocity core of −44.0 cm s^{-1} (Fig. 5a). The absolute geostrophic velocity sections, estimated from the CTD data at five PIES stations by referring to the ship-mounted ADCP velocity at 800 m (Fig. 5b) and from the GEM-derived hydrographic data and PIES pressure data as shown in Eqs. (1)–(6) (Fig. 5c), are similar to each other: both of them show a southwestward current with a strong surface velocity. Since the barotropic component of current is at an order of several cm/s, it is smaller than the baroclinic component (Fig. 5). The volume transports integrated over the section for Fig. 5a–c are −8.4, −8.0, and −8.1 Sv, respectively. Agreement of velocity structures and volume transports for Fig. 5a–c indicates that our volume transports estimated using the PIES-measured P_b and τ are likely reasonable.

During 22 months of PIES measurement, the velocity structure and associated volume transport derived from PIES-measured P_b and τ have a large variability. As two examples, the velocity was northeastward with a maximum velocity of 104.1 cm s^{-1} (volume transport 17.4 Sv) on 1

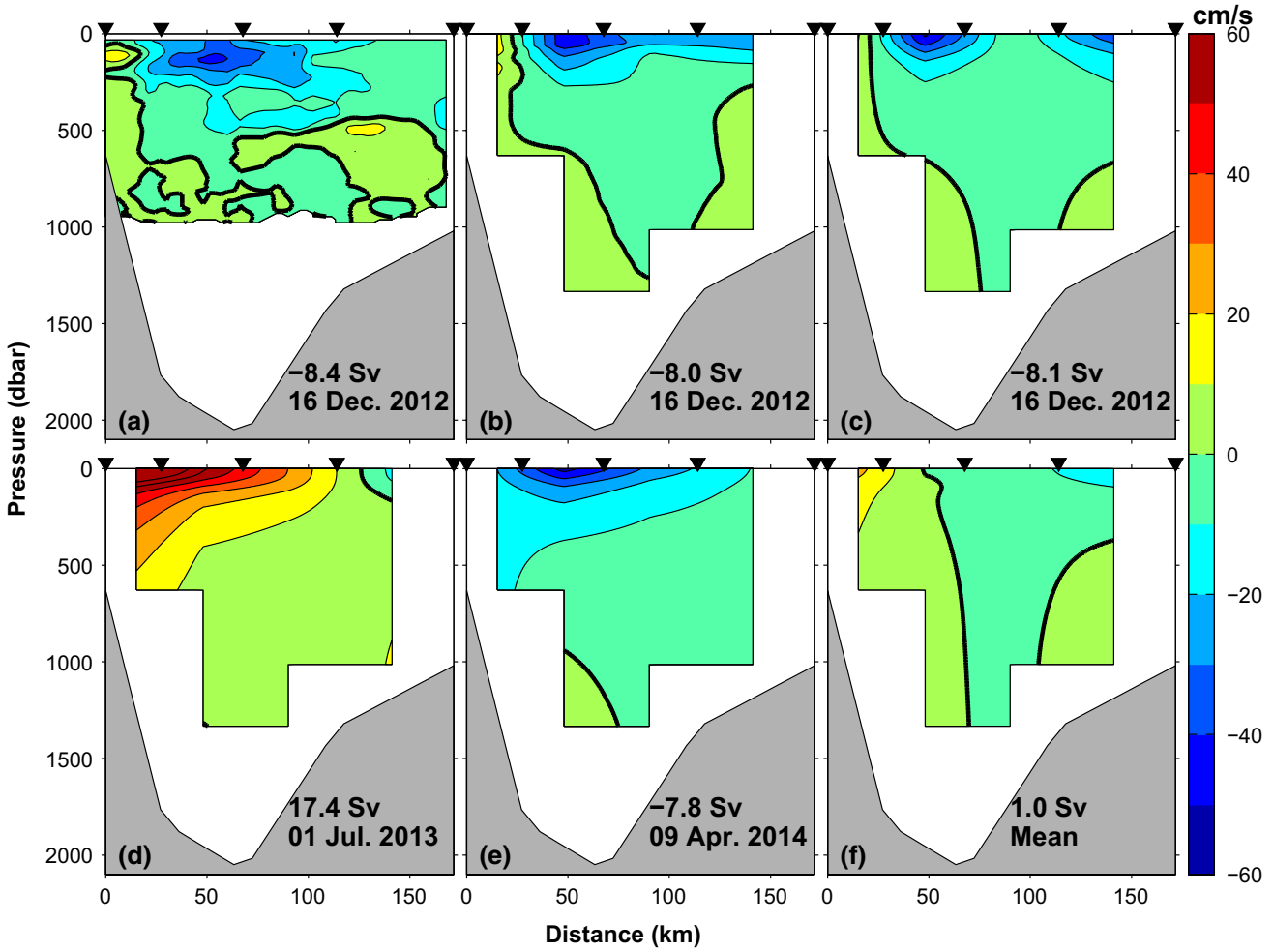

Fig. 5 Vertical distribution of velocity normal to the section for the mooring array: **a** measured by ship-mounted ADCP; **b** absolute geostrophic velocity estimated using the CTD data by referring to the ship-mounted ADCP velocity at 800 m; and PIES-derived geostrophic velocities estimated by using Eqs. (1)–(6) on **c** 16 December 2012, **d** 1 July 2013 when a warm-eddy arrived, **e** 9 April 2014 when a cold-eddy arrived; and **f** mean PIES-derived geostrophic velocity for the whole mooring period. *Positive* (*negative*) values indicate northeastward (southwestward) currents. Contour interval is 10 cm s^{-1}. *Thick line* shows zero velocity. *Triangles* on the top of each panel indicate the locations of the PIESs

July 2013 (Fig. 5d) and southwestward (volume transport −7.8 Sv) on 9 April 2014 (Fig. 5e). Combined with satellite altimeter data, we know the former case (Fig. 5d) corresponds to the arrival of a warm-eddy to the section while the latter case (Fig. 5e) to that of a cold eddy, that is, the velocity at the shelf slope of NSCS is strongly influenced by arrivals of mesoscale eddies. The 22-month mean velocity shows a weak northeastward current whose volume transport is 1.0 Sv (Fig. 5f).

3.2 Estimation of a 22-year volume transport time series

Using the mooring array data, we can estimate a 22-month volume transport time series (VT_{PIES}) from October 2012 to July 2014 across the section. However, this 22-month time series is not long enough to examine long-term variations and their statistical characters because the current during 22 months is strongly influenced by mesoscale eddies and the seasonal monsoon. To obtain a long-term volume transport time series, we established an empirical relationship between this 22-month volume transport time series and simultaneous satellite altimeter data following the methods that have been used previously for the Kuroshio and Ryukyu Current (Imawaki et al. 2001; Zhu et al. 2004; Andres et al. 2008a).

The satellite track of Pass 114 (blue dots in Fig. 1b) is a descending track passing five PIES sites. The satellite-measured sea surface height anomaly (SSHA) data along the track were first lowpass-filtered with a five-point filter

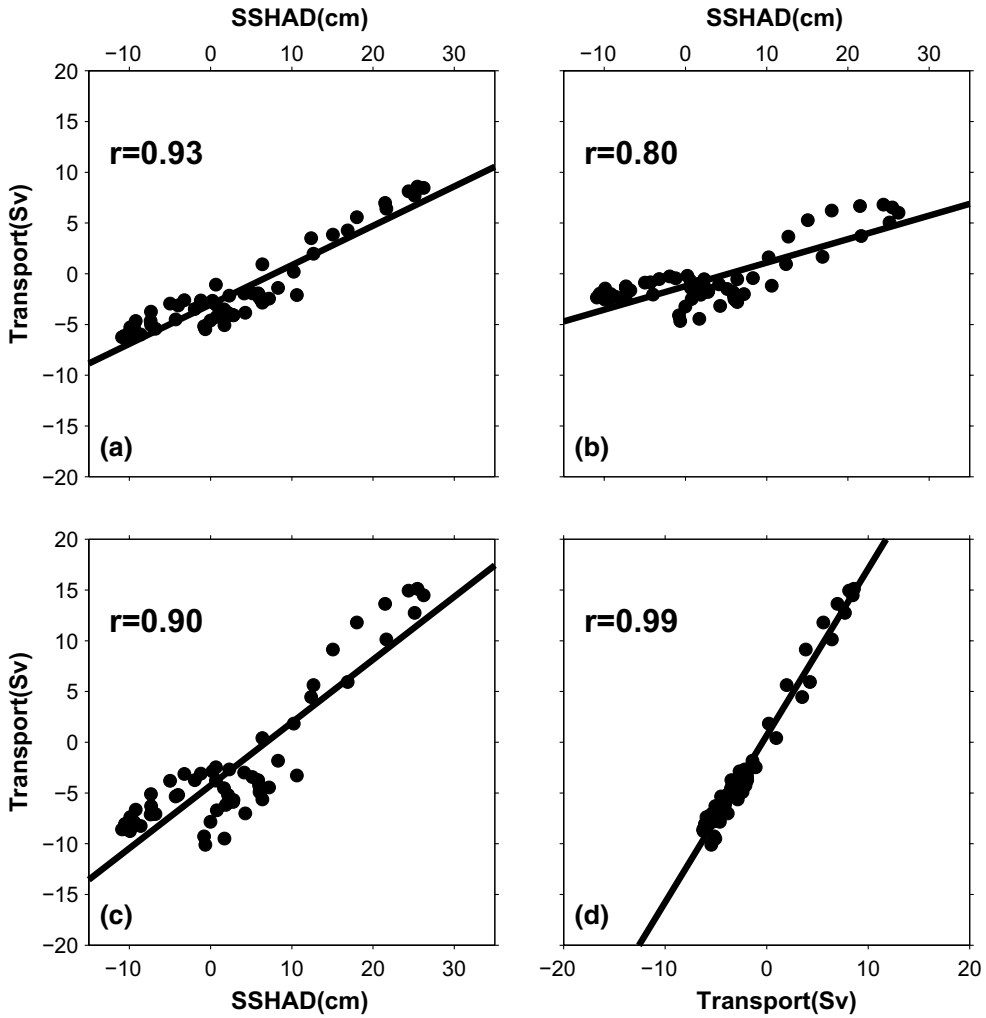

Fig. 6 *Scatter plots* of volume transport in **a** the upper 200 dbar, **b** the deep layer below 200 dbar and **c** the full-water-column transport against the sea surface height anomaly difference (SSHAD, unit: cm). **d** *Scatter plots* of volume transport in upper 200 dbar against the full-water-column transport. The correlation coefficient and the root-mean-square difference from the regression line are shown in the *upper-left corner* of each panel. The volume transport was estimated from PIES data and SSHAD was estimated from satellite altimeter data

corresponding to a spatial scale of about 29 km. The SSHA at each PIES site is highly correlated with τ measured by the PIES. The highest correlation coefficients were 0.91 and 0.92 at P1 and P5, respectively. The SSHA difference between P1 and P5 (ΔSSHA) is well correlated with the 40-day lowpass-filtered volume transport in the upper 200 dbar (correlation coefficient is 0.93) (Fig. 6a), and is also correlated with similarly filtered volume transport in the deep layer below 200 dbar (correlation coefficient is 0.80) (Fig. 6b). Because the volume transport in the upper 200 dbar is well correlated with the full-water-column transport (Fig. 6d), the ΔSSHA is, therefore, well correlated with the full-water-column transport (correlation coefficient is 0.90) (Fig. 6c). Using this empirical relationship, we then produce a 22-year time series of volume transport from 1992 to 2014. We refer to this volume transport time series as VT_{NSCS} (volume transport in the NSCS).

3.3 Variability of the VT_{NSCS}

The VT_{NSCS} time series is in good agreement with the VT_{PIES} time series (Fig. 7a). Their RMSD is 3.5 Sv, much smaller than the peak-to-peak range of about 25 Sv. The VT_{NSCS} time series is also in good agreement with the volume transport (VT_{HYCOM}) estimated from the 1/12° global Hybrid Coordinate Ocean Model (HYCOM) results (Bleck, 2002) (blue line in Fig. 7b) with a RMSD of 3.0 Sv. Consequently, our estimated VT_{NSCS} is likely reasonable.

During the 22 years, VT_{NSCS} fluctuates largely from -11.8 to 19.7 Sv, with a standard deviation of 5.3 Sv

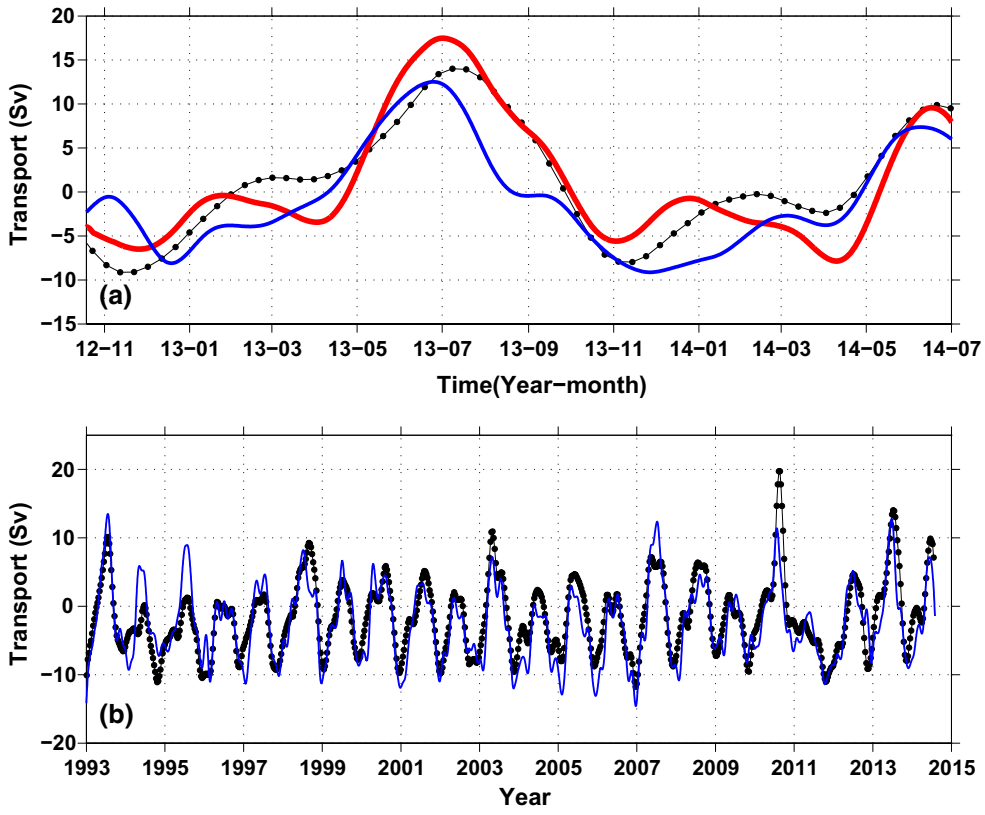

Fig. 7 **a** Time series of VT_{PIES} (*red line*), VT_{NSCS} (*dotted black line*), and VT_{HYCOM} (*blue line*) for the mooring period (October 2012–July 2014). **b** Time series of VT_{NSCS} (*dotted black line*) and VT_{HYCOM} (*blue line*) from January 1993 to December 2014 (color figure online)

(Fig. 7b). The 22-year mean VT_{NSCS} is −1.6 Sv, indicating a southwestward current. Maximum VT_{NSCS} occurred in August 2010, which was due to an exceptional anticyclonic eddy around Xisha Island (Chu et al. 2014). VT_{NSCS} typically has a positive value in the warm season and a negative value in the cold season, which indicates a monsoon cycle response of the SCS circulation.

The power spectrum of VT_{NSCS} shows the most prominent energy at the annual period (Fig. 8). Two peaks at about 605 and 875-day are between 90 % (thin broken line in Fig. 8) and 95 % (thick broken line in Fig. 8) confidence levels, suggesting the quasi-biennial oscillation occurred in the SCS, but were weaker than that in the North Pacific (Zhu et al. 2004). The power spectra of VT_{NSCS} show that the peak around 100-day period is not remarkable. This indicates that the mesoscale eddies with 100-day period, originating from the North Pacific Subtropical Countercurrent region (Qiu 1999) propagated westward (Yang et al. 1999; Zhu et al. 2004) may not arrive at the PIES sites or have been greatly weakened, possibly due to blocking by the northward-flowing Kuroshio as the eddies pass through the Luzon Strait.

Since the power spectrum of VT_{NSCS} shows the most prominent energy peak at the annual period, we average

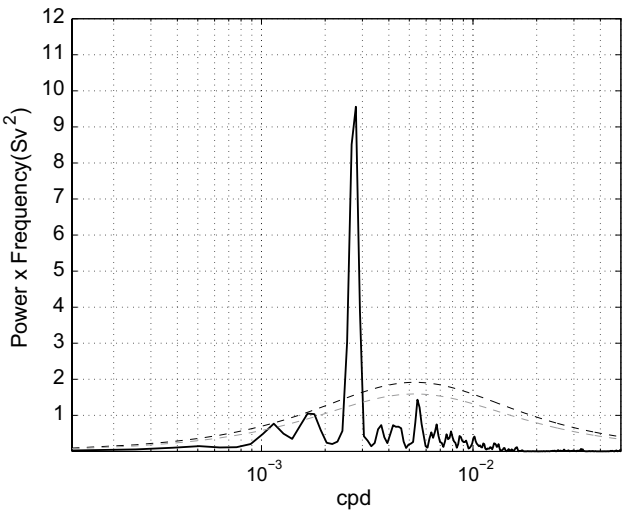

Fig. 8 Variance-preserving power spectrum of volume transports through the mooring array. *Thick* and *thin broken lines* indicate 95 and 90 % confidence levels based on the best-fit, first-order autoregressive model spectrum, respectively

and plot the 22-year VT_{NSCS} time series by month and by season to examine the annual cycle and seasonal variation. The monthly averaged VT_{NSCS} changes not only in

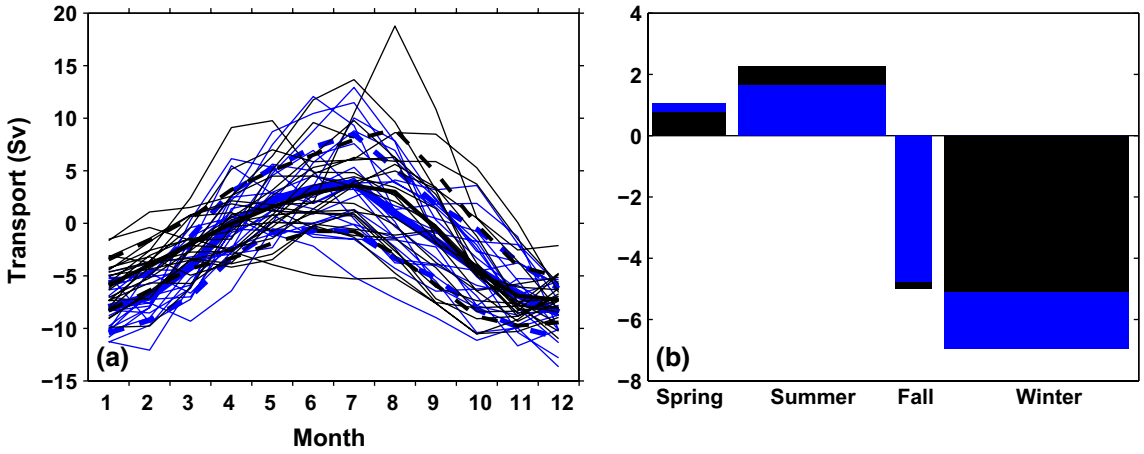

Fig. 9 **a** Monthly averaged VT_{NSCS} (*black lines*) and VT_{HYCOM} (*blue lines*) for the 22 individual years (*thin lines*) and averaged over all 22 years (*thick line*); the *two dashed lines* represent ±one standard deviation of VT_{NSCS} and VT_{HYCOM} for each month. **b** Seasonal means for VT_{NSCS} (*black*) and VT_{HYCOM} (*blue*) (color figure online)

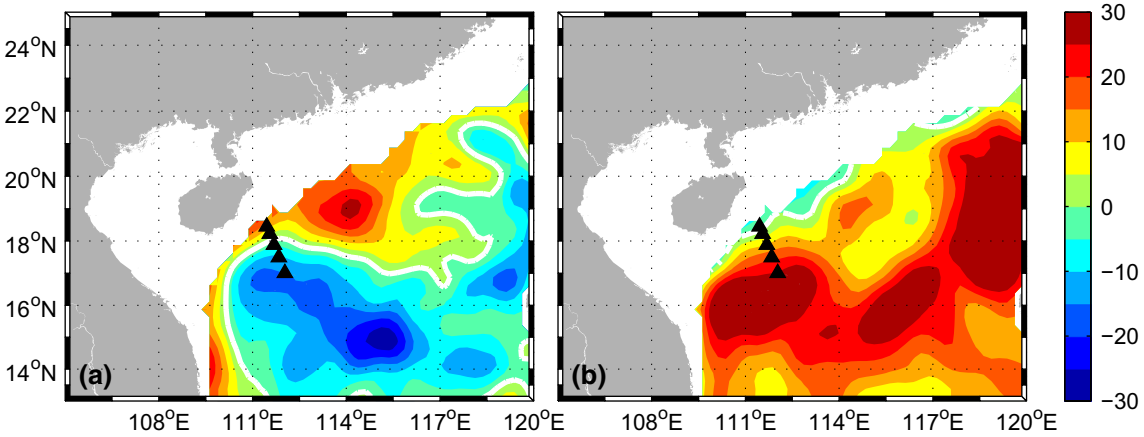

Fig. 10 SSHA (cm) distribution when the volume transports takes the minimum value and the maximum value in **a** 7 April 2013 and **b** 24 June 2014, respectively. The triangles in each panel indicate the PIES positions. The regions with depth shallower than 200 m are masked

magnitude but also in direction (Fig. 9a). The monthly averaged VT_{NSCS} has a maximum (3.6 Sv, northeastward) in July and a minimum (−7.3 Sv, southwestward) in December with a standard deviation of 3.6 Sv. The annual range (peak-to-peak difference) reaches 10.9 Sv (Fig. 9a). This annual range is larger than those of the Kuroshio in the East China Sea (Andres et al. 2008a) and south of Japan (Imawaki et al. 2001) and the Ryukyu Current southeast of Okinawa (Zhu et al. 2004), although its mean (−1.6 Sv) is much smaller than the means of Kuroshio and Ryukyu Current. The mean VT_{NSCS} values for spring (April–May), summer (June–September), fall (October to early November), and winter (November–March) are 0.8, 2.3, −5.0, and −5.1 Sv, respectively (Fig. 9b) (the season is defined following Fang et al. 2002).

The reversal date of mean VT_{NSCS} in spring when VT_{NSCS} changes from southwestward to northeastward is 8 April (thick black line in Fig. 9a), about 28 days after the reversal of wind direction over the SCS (figure not shown), while the reversal date of mean VT_{NSCS} in fall (from northeastward to southwestward) is 13 September, about 15 days after the reversal of wind direction in fall.

4 Summary and discussion

We successfully carried out a 22-month mooring deployment of five PIESs along a satellite altimeter track across the continental slope in the NSCS. Using the round-trip acoustic travel time data with the GEM method, we estimated the temperature profile time series at the five PIES

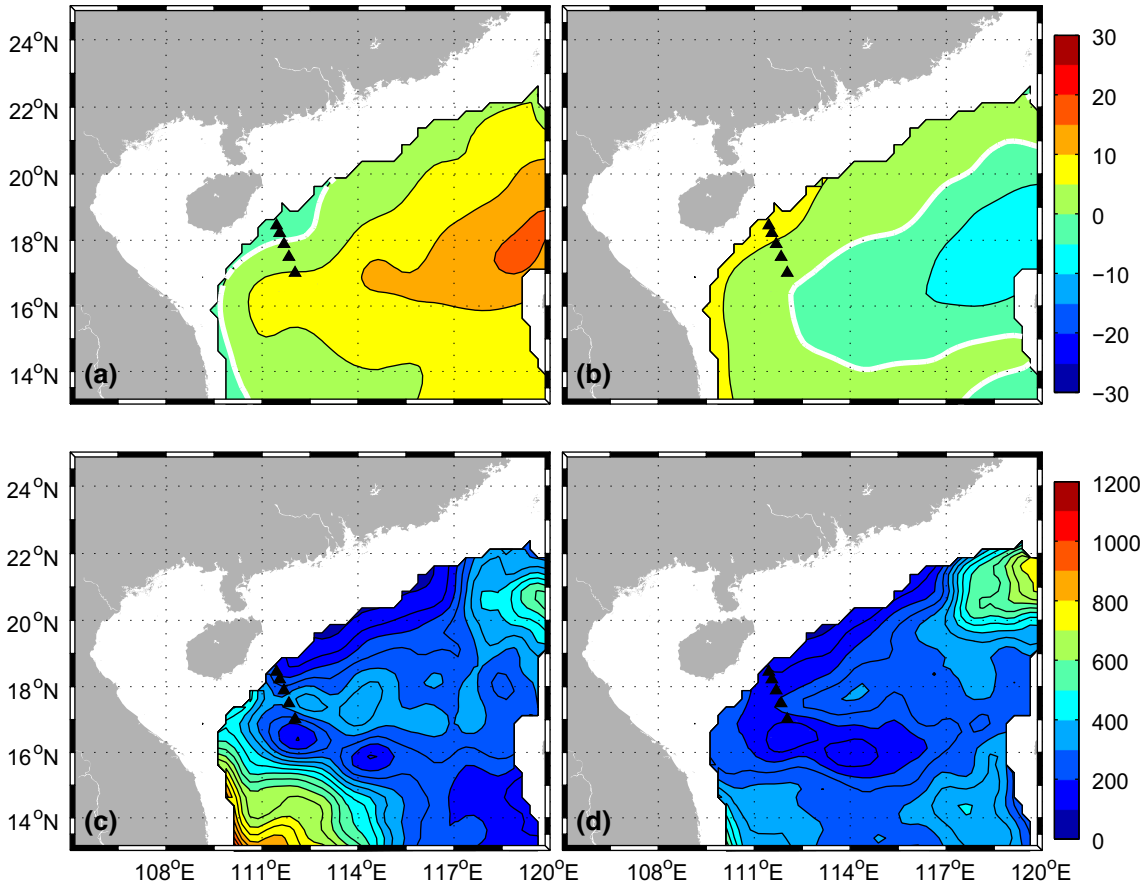

Fig. 11 SSHA distribution (cm) for **a** summer and **b** winter, and eddy kinetic energy ($cm^2\ s^{-2}$) distribution for **c** summer and **d** winter. The *triangles* in each panel indicate the PIES positions. The regions with depth shallower than 200 m are masked

stations. The GEM-inferred temperatures were in good agreement with those measured independently by the CTD casts at the five PIES stations during mooring period. Then, we calculated the absolute geostrophic velocity normal to the section and obtained a 22-month-long record of volume transports by combining the GEM-derived hydrographic data, PIES pressure data, and the ship-mounted ADCP velocity data.

By using this 22-month-long record of volume transport data with satellite altimeter data, we estimated a 22-year VT_{NSCS} in the NSCS and determined its mean and variability including the seasonal cycle and influence of mesoscale eddies. VT_{NSCS} showed a significant seasonal reversal with an annual range of 10.9 Sv, which is much larger than its mean (−1.6 Sv). Mesoscale eddies greatly impacted VT_{NSCS} with an upper range of about 20 Sv (Fig. 7b; in August 2010).

Currents near our mooring site are known to flow typically approximately along the isobaths of the SCS continental slope (Wang et al. 2013), but no previous studies have obtained time series of volume transport over the SCS. Our winter mean VT_{NSCS} (−5.1 Sv) is slightly larger than that (about −4 Sv) predicted by Liu et al. (2001) from Sverdrup theory using the monthly mean Comprehensive Ocean–Atmosphere Data Set (COADS) wind-stress curl over the SCS, while our summer mean VT_{NSCS} (2.3 Sv) is quite different from their prediction (about −3.5 Sv). This suggests that the seasonal variation of VT_{NSCS} in the NSCS may not exactly follow Sverdrup balance, because the SCS summer circulation is weak and more complicated than that in winter (Fang et al., 2012). Nevertheless, our summer VT_{NSCS} is the first long-term measurement evidence supporting the schematic circulation pattern in the NSCS, hypothesized by Fang et al. (2012) (see Fig. 3 in their paper). The mean VT_{NSCS} through fall and winter is about −5 Sv, larger in magnitude than the outflow transport through the Karimata Strait (3.6 Sv) in winter (Fang et al. 2010), which indicates that part of the VT_{NSCS} may flow out the SCS as a portion of the SCS throughflow, while some of the VT_{NSCS} joins the inner SCS circulation in the SCS.

The mesoscale eddies near the Xisha Island are mainly from the south, propagated from the east of Vietnam, and also from the east, propagated from the region near the

Luzon Strait (Wang et al. 2003, 2015). To examine how mesoscale eddies influence the VT_{NSCS}, we plot the SSHA distributions when the VT_{NSCS} reaches the minimum on 7 April 2013 (Fig. 10a) and the maximum on 24 June 2014 (Fig. 10b). When the VT_{NSCS} took the minimum (maximum) value, a cyclonic (anticyclonic) eddy extended to the southeast side of observation line, making the VT_{NSCS} southwestward (northeastward).

From the 22-year time series of VT_{NSCS}, it is known that Sverdrup balance does not fully explain the seasonality of the transport in summer. To examine the possible mechanism of the seasonal variability of VT_{NSCS}, we plot the mean SSHA and eddy kinetic energy distributions calculated using surface geostrophic velocity from SSHA data for summer and winter (Fig. 11). The SSHA distributions show a seasonal reversal structure corresponding to the southwestward and northeastward VT_{NSCS} in summer and winter, respectively. However, the eddy kinetic energy near our mooring area is relatively small and almost the same in the two seasons, indicating that the mesoscale eddies do not exhibit clearly seasonal variability. This means that effects of mesoscale eddies can be removed by averaging the 22-year-long data, and also implies that the mesoscale eddies may not be an important factor of seasonality of the VT_{NSCS}. The seasonal variability of the Kuroshio transport in the East China Sea also does not follow the Sverdrup theory, whose mechanism was explained as joint effect of baroclinicity and bottom relief (JEBAR; Kagimoto and Yamagata 1997). It is suggested that similar work, such as high-resolution numerical simulation, should be carried out to examine the possible mechanism of the seasonal variability in the SCS.

The methodology, using PIES near-bottom pressure data combined with ship-mounted ADCP data to estimate barotropic velocity, is applied here for the first time in a case lacking current meter measurements such as those provided by the current pressure-recording inverted echo sounder (Andres et al. 2008b; Donohue et al. 2010). The present method has its limitations due to formula approximations. The temporal-mean barotropic component velocity $\bar{V}_{bt}$, estimated in our geostrophic calculation using Eq. (6), were obtained from only single time ship-mounted ADCP measurement. The error of $\bar{V}_{bt}$ is expected to be smaller than the error of the ship-mounted ADCP (about 3 cm s^{-1}). We also note that the volume transport presented in this study is not the total volume transport of the SCS western boundary current, because our mooring array does not cover the area shallower than the water depth of P1 site (about 500 m, Fig. 1c). Nevertheless, the present study provides a useful long-term volume transport time series based on in situ observation data, which will be opened to the community in a near future (http://www.scs-data.icoc.cc/).

Acknowledgments This study is supported by the National Basic Research Program of China (2011CB403503), the National Natural Science Foundation of China (41276095, 41476020, 41276028, and 41321004), the Scientific Research Fund of SIO under grants JT1402 and JT1207, and the projects of State Key Laboratory of Satellite Ocean Environment Dynamics, Second Institute of Oceanography (SOEDZZ1403), and Global Change and Air-Sea Interaction (GASI-03-01-01-02). The Argo data are provided by China Argo Real-time Data Center (http://www.argo.gov.cn/argo-eng/index.asp). The HYCOM data are downloaded from http://hycom.org/. We thank the crew and participants of the R/V Shiyan-3 for their support during deployment cruise.

References

Andres M, Park JH, Wimbush M, Zhu XH, Chang KI, Ichikawa H (2008a) Study of the Kuroshio/Ryukyu Current system based on satellite-altimeter and in situ measurements. J Oceanogr 64(6):937–950

Andres M, Wimbush M, Park JH, Chang KI, Lim BH, Watts DR, Ichikawa H, Teague WJ (2008b) Observations of Kuroshio flow variations in the East China Sea. J Geophys Res 113:C05013. doi:10.1029/2007JC004200

Bleck R (2002) An oceanic general circulation model framed in hybrid isopycnic-Cartesian coordinates. Ocean Modell 4:55–88

Chu X, Xue H, Qi Y, Chen G, Mao Q, Wang D, Chai F (2014) An exceptional anticyclonic eddy in the South China Sea in 2010. J Geophys Res Oceans 119:881–897. doi:10.1002/2013JC009314

Donohue KA, Watts DR, Tracey K, Greene AD, Kennelly M (2010) Mapping circulation in the Kuroshio Extension with an array of current and pressure recording inverted echo sounders. J Atmos Oceanic Technol 27:507–527. doi:10.1175/2009JTECHO686.1

Fang W, Fang G, Shi P, Huang Q, Xie Q (2002) Seasonal structures of upper layer circulation in the southern South China Sea from in situ observations. J Geophys Res 107(C11):3202. doi:10.1029/2002JC001343

Fang G, Wang Y, Wei Z, Fang Y, Qiao F, Hu X (2009) Interocean circulation and heat and freshwater budgets of the South China Sea based on a numerical model. Dyn Atmos Oceans 47:55–72. doi:10.1016/j.dynatmoce.2008.09.003

Fang G, Susanto RD, Wirasantosa S, Qiao F, Supangat A, Fan B, Wei Z, Sulistiyo B, Li S (2010) Volume, heat, and freshwater transports from the South China Sea to Indonesian seas in the boreal winter of 2007–2008. J Geophys Res 115:C12020. doi:10.1029/2010JC006225

Fang G, Wang G, Fang Y, Fang W (2012) A review on the South China Sea western boundary current. Acta Oceanol Sin 31(5):1–10. doi:10.1007/s13131-012-0231-y

Hsin YC, Wu CR, Chao SY (2012) An updated examination of the Luzon Strait transport. J Geophys Res 117:C03022. doi:10.1029/2011JC007714

Hu J, Kawamura H, Li C, Hong H, Jiang Y (2010) Review on current and seawater volume transport through the Taiwan Strait. J Oceanogr 66:591–610

Imawaki S, Uchida H, Ichikawa H, Fukasawa M, Umatani S, ASUKA Group (2001) Satellite altimeter monitoring the Kuroshio transport south of Japan. Geophys Res Lett 28:17–20

Kagimoto T, Yamagata T (1997) Seasonal transport variations of the Kuroshio: an OGCM simulation. J Phys Oceanogr 27:403–418

Liu ZY, Yang HJ, Liu QY (2001) Regional dynamics of seasonal variability of SSH in the South China Sea. J Phys Oceanogr 31:272–284

Qiu B (1999) Seasonal eddy field modulation of the North Pacific Subtropical Countercurrent: TOPEX/Poseidon observation and theory. J Phys Oceanogr 29:2471–2486

Qu T, Song YT (2009) Mindoro Strait and Sibutu Passage transports estimated from satellite data. Geophys Res Lett 36:L09601. doi:10.1029/2009GL037314

Qu T, Du Y, Sasaki H (2006) South China Sea throughflow: a heat and freshwater conveyor. Geophys Res Lett 33:L23617. doi:10.1029/2006GL028350

Wang G, Su J, Chu PC (2003) Mesoscale eddies in the South China Sea observed with altimeter data. Geophys Res Lett 30(21):2121. doi:10.1029/2003GL018532

Wang D, Liu Q, Huang RX, Du Y, Qu T (2006) Interannual variability of the South China Sea throughflow inferred from wind data and an ocean data assimilation product. Geophys Res Lett 33:L14605. doi:10.1029/2006GL026316

Wang D, Wang Q, Zhou W, Cai S, Li L, Hong B (2013) An analysis of the current deflection around Dongsha Islands in the northern South China Sea. J Geophys Res Oceans 118:490–501. doi:10.1029/2012JC008429

Wang Q, Zeng L, Zhou W, Xie Q, Cai S, Yao J, Wang D (2015) Mesoscale eddies cases study at Xisha waters in the South China Sea in 2009/2010. J Geophys Res Oceans 120:517–532. doi:10.1002/2014JC009814

Watts DR, Sun C, Rintoul S (2001) A two-dimensional gravest empirical mode determined from hydrographic observations in the Subantarctic Front. J Phys Oceanogr 31:2186–2209. doi:10.1175/1520-0485(2001)031,2186:ATDGEM.2.0.CO;2

Wu CR, Shaw PT, Chao SY (1998) Seasonal and interannual variations in the velocity field of the South China Sea. J Oceanogr 54(4):361–372

Wyrtki K (1961) Physical oceanography of the Southeast Asian waters, scientific results of marine investigations of the South China Sea and the Gulf of Thailand. NAGA Report. Scripps Inst Oceanogr 2:195 **(La Jolla, CA)**

Yang Y, Liu CT, Hu JH, Koga M (1999) Taiwan Current (Kuroshio) and impinging eddies. J Oceanogr 55:609–617

Zhu XH, Han IS, Park JH, Ichikawa H, Murakami K, Kaneko A, Ostrovskii A (2003) The northeastward current southeast of Okinawa Island observed during November 2000 to August 2001. Geophys Res Lett 30(2):1071. doi:10.1029/2002GL015867

Zhu X-H, Ichikawa H, Ichikawa K, Takeuchi K (2004) Volume transport variability southeast of Okinawa Island estimated from satellite altimeter data. J Oceanogr 60:953–962